

MRC B1221–423: a compact steep-spectrum radio source in a merging galaxy^{*}

Helen M. Johnston,^{1,†} Richard W. Hunstead¹, Garret Cotter^{2,3} and Elaine M. Sadler¹

¹*School of Physics, University of Sydney, NSW 2006, Australia*

²*Cavendish Laboratory, Madingley Road, Cambridge CB3 0HE*

³*Department of Astrophysics, University of Oxford, Keble Road, Oxford OX1 3RH*

Received:

ABSTRACT

We present *BVR*IK images and spectroscopic observations of the $z = 0.17$ host galaxy of the compact steep-spectrum radio source MRC B1221–423. This is a young ($\sim 10^5$ yr) radio source with double lobes lying well within the visible galaxy. The host galaxy is undergoing tidal interaction with a nearby companion, with shells, tidal tails, and knotty star-forming regions all visible. We analyse the images of the galaxy and its companion pixel-by-pixel, first using colour-magnitude diagrams, and then fitting stellar population models to the spectral energy distributions of each pixel. We also present medium-resolution spectroscopy of the system.

The pixels separate cleanly in colour-magnitude diagrams, with pixels of different colours occupying distinct regions of the host galaxy and its companion. Fitting stellar population models to these colours, we have estimated the age of each population. We find three distinct groups of ages: an old population ($\tau \sim 15$ Gyr) in the outskirts of the host galaxy; an intermediate-age population ($\tau \sim 300$ Myr) around the nucleus and tidal tail, and a young population ($\tau \lesssim 10$ Myr) in the nucleus and blue “knots”.

The spectrum of the nucleus shows numerous strong emission lines, including [O I] $\lambda 6300$, [O II] $\lambda 3727$, [S II] $\lambda \lambda 6716, 6731$, $H\alpha$, and [N II] $\lambda \lambda 6548, 6583$, characteristic of a LINER spectrum. The companion galaxy shows much narrower emission lines with very different line ratios, characteristic of a starburst galaxy.

We have evidence for three distinct episodes of star formation in B1221–423. The correlation of age with position suggests the two most recent episodes were triggered by tidal interactions with the companion galaxy. The evidence points to the AGN in the centre of B1221–423 having been “caught in the act” of ignition. However, none of the components we have identified is as young as the radio source, implying that the delay between the interaction and the triggering of the AGN is at least 3×10^8 years.

Key words: Galaxies: active — galaxies: interactions — galaxies: stellar content

1 INTRODUCTION

The onset of AGN activity in galaxies appears to be closely related to starbursts, possibly triggered by mergers, which lead to large increases in the amount of material being fed to the central black hole, thereby triggering the radio emission. Many radio galaxies show signatures of tidal interactions, such as tails, bridges, shells, and double nuclei (see Barnes & Hernquist 1992, for a review). HST observations of powerful radio galaxies at

$z \sim 1$ show disturbed, knotty rest-frame UV emission in the host galaxies (Longair, Best & Röttgering 1995; Best, Longair & Röttgering 1996).

Compact steep-spectrum (CSS) sources are bright but compact radio galaxies, with sizes 1–20 kpc. Unlike the majority of powerful radio galaxies, the radio source is wholly contained within the envelope of the host galaxy. They have a steep spectral index, $\alpha < -0.5$ ($S_\nu \propto \nu^\alpha$), and a radio spectrum peaking below 500 MHz. CSS sources are powerful ($P_{1.4} \gtrsim 10^{25}$ W Hz⁻¹), and make up about 20% of bright flux-limited low-frequency radio catalogues like the 3CR catalogue (Bennett 1962) or the Molonglo Reference Catalogue (Large et al. 1981). They typically have redshifts between 0.1–2 (see O’Dea 1998, for a review). The two competing

^{*} Based on observations made with ESO Telescopes at the La Silla Observatory, programs 70.A-0387(A) and 66.A-0288(B)

[†] E-mail: H.Johnston@physics.usyd.edu.au

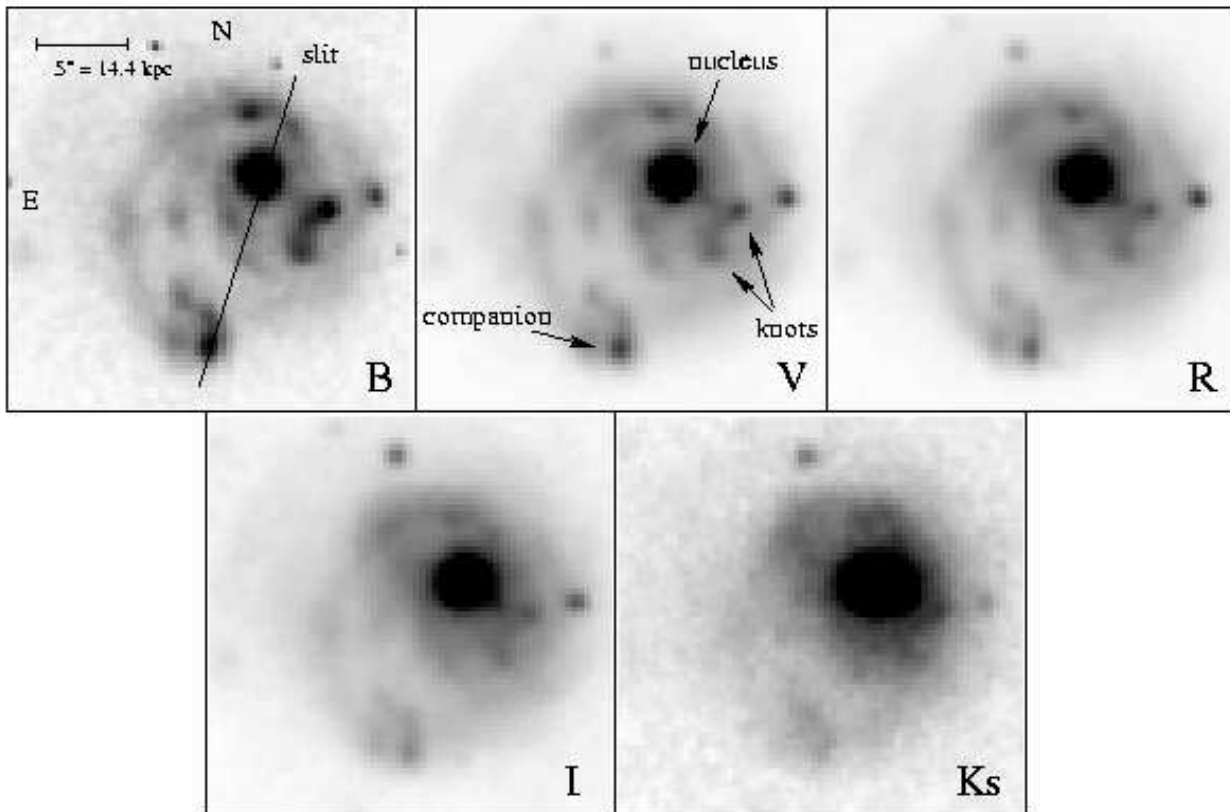


Figure 1. *BVRKI* images of MRC B1221–423. Knots of star-formation and a tidal tail joining the galaxy to the companion are clearly visible. The size of each image is 22 arcsec; the separation of the galaxy and the companion is 10 arcsec (1 arcsec = 2.88 kpc assuming $H_0 = 71 \text{ km s}^{-1} \text{ Mpc}^{-1}$ and $\Omega_M = 0.27$). The orientation of the slit for the spectroscopic observations (PA = $-18^\circ 5$) is shown as the line joining the galaxy to the companion on the *B* image. The labels on the *V* band image indicate the various regions described in the text.

models for CSS sources are (a) that they are small in size because the jets are “frustrated” by interaction with dense surrounding gas; and (b) that they are young sources which will eventually evolve into classical large double-lobed radio sources (O’Dea 1998). Most evidence suggests that CSS sources are young (e.g. Fanti et al. 1990), and will fade as they grow into large-scale radio sources. Significant luminosity evolution is required to explain the fact that the age of CSS sources is only 1% that of the large radio sources, yet 20% or more of bright centimetre-wavelength-selected samples are CSS sources (e.g. Scheuer 1974; Kaiser & Alexander 1997; Readhead et al. 1996). The best evidence for the youth of CSS sources is the detection of hotspot advance speeds of 0.1 to $0.3c$ in compact symmetric objects (see Conway 2002, and references therein).

MRC B1221–423 is one of the nearest CSS sources, located in a host galaxy with a redshift $z = 0.1706$ (Simpson et al. 1993). The radio source has a steep spectrum ($\alpha = -0.85$) and double lobes with a separation of only $1''.5$, which lie well within the envelope of the visible galaxy (Safouris, Hunstead & Prouton 2003). The structure is suggestive of the lobes seen in larger double sources; there is no evidence of a core. Safouris et al. (2003) estimated the age of the radio source to be 10^5 yr, using the tight correlation between the total kinetic power of the jet and the

narrow-line luminosity (Rawlings & Saunders 1991). At the distance of the galaxy, 1 arcsec corresponds to a distance of 2.876 kpc, assuming $H_0 = 71 \text{ km s}^{-1} \text{ Mpc}^{-1}$ and $\Omega_M = 0.27$.

The host galaxy is highly disturbed, showing signs of tidal interaction with at least one close companion. An archival image taken using the Anglo-Australian Telescope in $1''.4$ seeing shows faint concentric arcs to the north-east (Safouris et al. 2003), evidence of past tidal interaction.

We have obtained multi-colour images of MRC B1221–423 in order to study the change in properties of the stellar population across the galaxy. The use of spatially-resolved colours to study differences in stellar populations across a galaxy has been shown to be an effective way to study age distributions, localised extinction and star formation history in galaxies. The technique was pioneered by Bothun (1986), who used a spatially resolved (*B* – *R*) vs. *B* diagram to examine the star formation history of NGC 4449. More recently, Abraham et al. (1999) used pixel colour-magnitude diagrams to investigate the evolutionary history of galaxies in the *Hubble Deep Field*, while Kong et al. (2000), de Grijs et al. (2003) and Kassin et al. (2003) used such diagrams to study various nearby galaxies.

In this paper, we present and analyse five-colour images and optical spectroscopic observations of MRC B1221–423.

In §2 we describe the observations and their reduction. In §3.1, we analyse the images, first by means of colour-magnitude diagrams, and then by fitting spectral energy distributions to each pixel. In § 3.2 we examine the surface-brightness profile of the galaxy. In §3.3 we discuss the spectroscopic results, and then discuss the implications for the history of the galaxy in §4.

2 OBSERVATIONS

2.1 Imaging

Four-colour optical images were taken on 2002 February 25 using SUSI2 on the New Technology Telescope (NTT) of the European Southern Observatory with Bessell *B*, *V*, *R* and *I* filters (Bessell 1990). The spatial scale on the detector (two 2k × 4k EEV CCDs) is 0.161 arcsec/pixel. The conditions were photometric, and details of the observations are given in Table 1. The equatorial standard star field PG0942 from Landolt (1992) was observed to derive the photometric transformations onto the Johnson-Cousins system. Standard reductions were performed using the IRAF software suite.

An infrared image was obtained on 2002 December 23 through the *Ks* filter using the SofI instrument on the NTT. The field of view using the Large Field objective was 4.9 arcmin, with a spatial scale of 0.292 arcsec/pixel. The auto-jitter mode was used to obtain fifteen separate images, with each image being an average of nine 7-s images; thus the total exposure time on source was 945 s. The telescope was moved by a random amount within a 100 arcsec box between images. Reduction of the images was done using the XDIMSUM¹ package in IRAF. The data were flattened using a sky flat created by masking out sources and combining the masked images; the final mosaic was then created using *xmosaic*. The Persson standard star SJ 9154 (Persson et al. 1998) was used to derive the photometric transformation.

Finally, all five images were registered onto the same pixel scale, by fitting the positions of stars common to each image with linear transformations, including terms for translation and scaling. The *Ks*-band image was re-binned to the same scale, and a term for rotation also included. The images were convolved with gaussians to match the image size on the worst-seeing image (the *Ks*-band image, with measured FWHM of 1.0 arcsec), and then binned 3 × 3, so the pixel scale of the final images is 0.483 arcsec/pixel, which critically samples the seeing disk. The registration of the images is accurate to about 0.2 pixels, as measured from the positions of field stars in the final images.

The final set of images is shown in Figure 1. The *B*-band samples rest-frame wavelengths in the range 3340–4180 Å, or essentially rest-frame *U*-band.

2.2 Spectroscopy

MRC B1221–423 was observed on four occasions, in 2001 April and 2003 August, using the Double Beam Spectro-

Table 1. Journal of observations of MRC B1221–423. The imaging observations were taken with the New Technology Telescope at the European Southern Observatory; the spectroscopic observations were taken using the Double Beam Spectrograph on the ANU 2.3m telescope at Siding Spring Observatory. The columns show the date of the observation, the wavelength range and the resolution in each of the spectrograph arms, and the exposure time. The seeing for the spectroscopic observations was 1''2–1''5.

| <i>Imaging observations</i> | | | | | |
|-----------------------------------|---------------------|-----------|-------------------------|---------------|-------------------------|
| UT Date | Instrument | Filter | t_{exp} (s) | Seeing (") | |
| 2002 Feb 25 | SUSI2 | <i>B</i> | 600 | 0.9 | |
| | | <i>V</i> | 600 | 0.7 | |
| | | <i>R</i> | 400 | 0.6 | |
| | | <i>I</i> | 900 | 0.8 | |
| 2002 Dec 23 | SofI | <i>Ks</i> | 945 | 1.0 | |
| <i>Spectroscopic observations</i> | | | | | |
| UT Date | λ range (Å) | | FWHM (Å) | | t_{exp} (s) |
| | blue | red | blue | red | |
| 2001 Apr 16 | 3180–5800 | 5880–7510 | 4.6 | 2.3 | 7200 |
| 2001 Apr 17 | 3180–5800 | 6610–8550 | 4.6 | 2.3 | 5400 |
| 2001 Apr 18 | 3180–5800 | 6610–8550 | 4.6 | 2.3 | 5400 |
| 2003 Aug 3 | 3180–10370 | – | 9.7 | – | 2400 |

graph on the ANU 2.3-m telescope at Siding Spring Observatory. The detectors were two SITe 1752 × 532 CCDs with 15- μ m pixels. A complete log of observations is given in Table 1. For the observations in 2001, a dichroic filter with a cross-over wavelength of 5500 Å was used to split the light into the two arms of the spectrograph. The observation in 2003 August was made with a low resolution grating and a plane mirror in place of the dichroic, so that all the light was sent to the blue arm of the spectrograph in order to obtain complete spectral coverage. Pairs of 1200 s or 1800 s exposures were bracketed with CuAr arc-lamp exposures. A slit of width 1.5 or 2 arcsec was used, oriented at a position angle of $-18^\circ.5$ so as to include light from the companion on the slit. On 2001 April 16, the position angle was -16° . The spatial scale on the detector was 0''.91/pixel, corresponding to a linear scale of 2.6 kpc per pixel.

The IRAF software suite was used to remove the bias and pixel-to-pixel gain variations from each frame. As we had multiple consecutive observations of the same object, cosmic ray events were removed using the technique described by Croke (1995), as implemented in FIGARO. The spectra were straightened in FIGARO so that the dispersion ran exactly along rows of the image, then a two-dimensional wavelength fit was performed to the arc images by fitting a third-order polynomial to the arc wavelengths as a function of pixel number, for each row of the image. These wavelength solutions were copied to the object images, interpolating between the bracketing arc exposures, and the data were re-binned so the wavelength-pixel relation was linear and uniform across the image. The sky background was subtracted from each image, by fitting to the sky on either side of the galaxy, chosen to be well outside the wings of the galaxy profile. The spectra were corrected for atmospheric extinction, the telluric absorption features were removed by comparing with the spectrum of a smooth-spectrum standard taken at similar airmass, and the spectra were flux-calibrated. The

¹ DIMSUM is the Deep Infrared Mosaicing Software package developed by Peter Eisenhardt, Mark Dickinson, Adam Stanford, and John Ward, and is available via ftp from <ftp://iraf.noao.edu/iraf/extern/dimsum/>

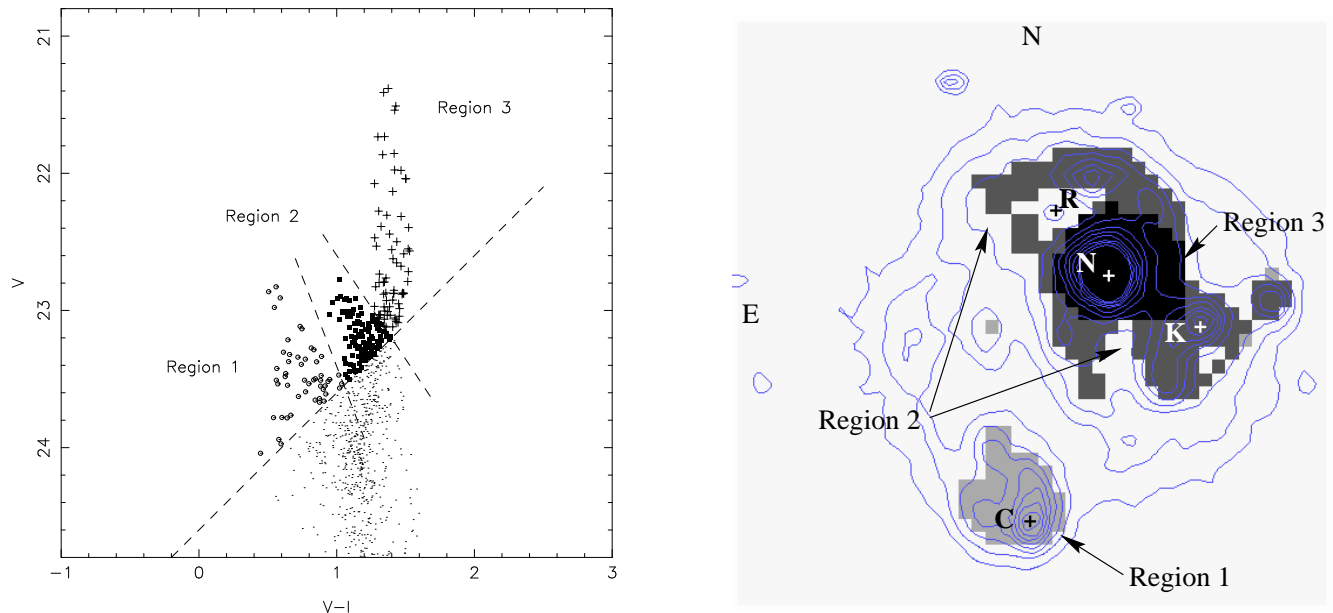


Figure 2. (a) V vs. $V - I$ colour-magnitude diagram for individual pixels in B1221–423. The units are magnitudes per pixel, where each pixel is 0.483 arcsec on a side. All pixels brighter than $V = 25$ are shown as dots. Three distinct “plumes” of pixels are seen; these correspond to the three regions in (b). The sky brightness was $V = 22.8$ mag pixel $^{-1}$. The dashed line shows the relation $(V - I) + V = 24.6$ mag, which we took as the boundary delimiting the regions. (b) Image showing the three regions identified in the colour-magnitude diagram, overlain with contours of the B -band image (Fig. 1). Light grey pixels are from region 1, dark grey from region 2, and black from region 3. The letters refer to model spectra shown in Fig. 4, representing pixels in the nucleus (N), companion (C), knot (K) and a red region to the north-east of the nucleus (R).

nights were not all photometric, so the flux calibration can only be regarded as approximate.

3 ANALYSIS

3.1 Modelling pixel colours

3.1.1 Colour-magnitude diagrams

Having created a uniform set of images, with the same scale, orientation and seeing, we can now use this dataset to study the variation in the stellar population across the face of the galaxy.

The pixel colours were first corrected for Galactic extinction, using the extinction map of Schlegel, Finkbeiner & Davis (1998), which indicates $A_V = 0.331$ mag at the position of MRC B1221–423. The other wavebands were corrected using the reddening law of Rieke & Lebofsky (1985). The $(V - I)$ vs. V colour-magnitude diagram for individual pixels of MRC B1221–423 is shown in Figure 2(a). Three distinct “plumes” of pixels are apparent in this diagram. We have mapped these three features, bounded on the lower edge by pixels satisfying the relation $(V - I) + V \leq 24.6$ mag, onto the image. This defines three distinct regions, shown in Figure 2(b). The features in the colour-magnitude diagram are clearly separate in the image. Pixels in the bluest region, Region 1, correspond to the interacting companion, with a hint of a trail of pixels back up the tidal tail (light grey pixels in Figure 2(b)). The reddest pixels, Region 3, come from the centre of the galaxy (black pixels); while the intermediate plume of pixels, Region 2, corresponds

to regions at larger radial distance from the centre of the galaxy, including the “knots” in the B -band image (dark grey pixels).

The lower boundary line in Figure 2(a) is arbitrary, and was chosen to show clearly the spatial separation of pixels of similar colours. Other features, such as the tidal tail, also occupy distinct regions of the colour-magnitude diagram, though the separation becomes blurred as the pixel flux density drops significantly below the sky level (22.8 mag per pixel in the V band). The same separation is seen for other colour-magnitude combinations, but is strongest for widely-separated bands.

Thus the colour-magnitude diagram separates pixels into distinct groups, with different regions of the diagram occupying different areas of the galaxy and its interacting companion. The most obvious interpretation of this effect is that the different groups represent different stellar populations; in this case, the three groups we define here probably represent the products of three distinct episodes of star formation.

3.1.2 Fitting spectral energy distributions

A colour-magnitude diagram does not use all the information we have available. With five colours, we can go further in analysing the stellar population: by fitting spectral models to the colours of each pixel in turn, we can determine the age and reddening of the stellar population across the face of the galaxy.

We used a purpose-written program to model the spectral energy distribution (SED) of pixels, loosely based on the HYPERZ code of Bolzonella, Miralles & Pelló (2000). The

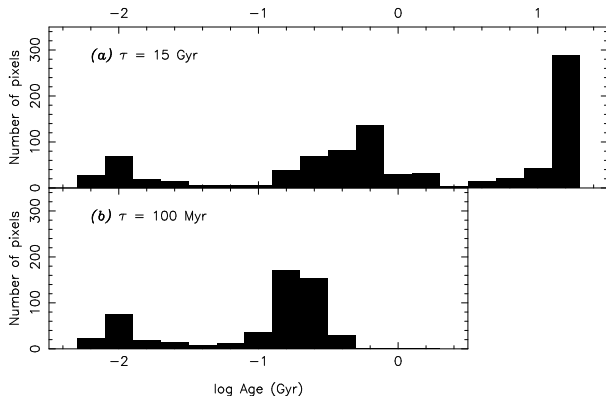


Figure 3. Histogram of ages for each pixel, derived from the best-fit model. The top panel shows ages derived from a model with exponentially decaying star formation with a decay time of $\tau = 15$ Gyr. The pixels are grouped into three distinct peaks, with ages of roughly 13 Gyr, 500 Myr and 10 Myr. The bottom panel shows a fit (excluding the pixels in the 15 Gyr peak) using a model with $\tau = 100$ Myr. The two young populations are still present, with ages around 210 Myr and 10 Myr.

method is as follows. An input stellar population model is chosen, and the redshift is fixed at the known redshift of the galaxy, $z = 0.1706$. A set of model spectral energy distributions is constructed by folding the input spectrum through the *BVR*IK response functions, resulting in a grid of model fluxes, with varying age and reddening along the axes, to be compared to the observed *BVR*IK fluxes for each pixel. The difference between the sum of the model fluxes and the observed fluxes in each bandpass is computed, and the parameters of the best fit (age and reddening) recorded.

Motivated by the work of Kassin et al. (2003) in modelling the stellar populations in the merging galaxies known as the “Antennae”, we used as our initial model an old star-forming disk model with exponentially decaying star formation on a timescale of $\tau = 15$ Gyr. The model was from the GISEL96 library (Bruzual & Charlot 1993), with a Salpeter initial mass function with mass limits of 0.1 and $100 M_{\odot}$ and solar metallicity, using the Gunn & Stryker (1983) stellar spectral atlas. A histogram of the fitted ages shows three distinct peaks, with ages of 13 Gyr, 500 Myr, and 10 Myr (Figure 3). We can refine this by fitting a model with $\tau = 100$ Myr to the “young” pixels, excluding those with ages above 5 Gyr (Figure 3, lower panel). The young pixels still show two distinct age groupings, with ages of 210 Myr and 10 Myr and younger.

Examples of the fitted spectral energy distributions are shown in Figure 4. The observed spectral energy distributions for the four points indicated with crosses in Figure 2(b) are plotted, together with the best-fit model spectra from the dual-age fit described above. Point R is in the “old” region, as indicated by the fit with the $\tau = 15$ Gyr model; the other three points were fitted using the $\tau = 100$ Myr model. The fitted parameters are shown in Table 2.

We can examine the location of the populations of different ages by plotting an age map of the galaxy. This is shown in Figure 5. The ages of pixels clearly correlate with morphological features of the galaxy (shown as contours for comparison). The old population is found through most of the galaxy, and clearly represents the underlying stellar pop-

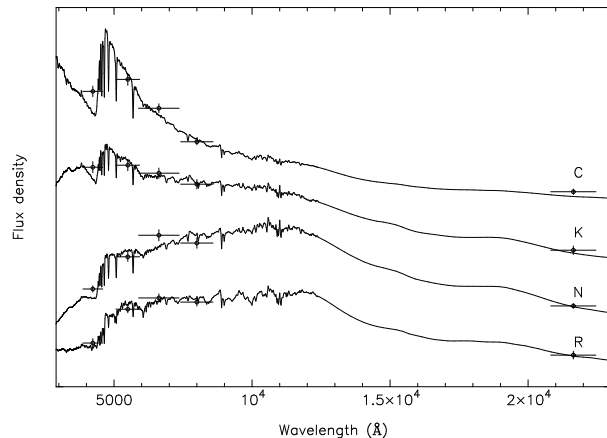


Figure 4. Spectral models fitted to observed spectral energy distributions, for the four points denoted with a letter in Figure 2(b), and an exponentially-decaying star-formation model fitted, as described in the text. The squares represent the pixel fluxes to which the model SEDs are fitted. The horizontal bars represent the widths of the filters, the vertical bars the photometric errors on the pixel fluxes. The spectra are offset in the vertical direction for clarity. The pixels shown are labelled with letters in Figure 2(b); they represent pixels in the companion (C), one of the blue knots to the west of the nucleus (K), the nucleus (N), and a red region to the north-east of the nucleus (R). The parameters of the fit are shown in Table 2.

Table 2. Parameters of the fits to the spectral energy distributions for the four selected points shown in Figure 2(b): the fits are shown in Figure 4. We fitted an exponentially-decaying star formation model with a timescale of either $\tau = 15$ Gyr or $\tau = 100$ Myr, as shown in the second column. The best-fit age and reddening for each set of pixel fluxes is shown in columns 3 and 4.

| Region | Model | Age (Myr) | A_V (mag) |
|------------|---------|--------------|----------------|
| Companion | 100 Myr | 290 | 0.1 |
| Knot | 100 Myr | 28 | 1.5 |
| Nucleus | 100 Myr | 128 | 2.0 |
| Red region | 15 Gyr | 15500 | 0.6 |

ulation of MRC B1221–423. The intermediate age population, with ages around 500 Myr, is found in the companion and along the tidal tail joining the galaxy to the companion, while the youngest population, with ages ~ 10 Myr, is found in the centre of MRC B1221–423 and in the knots surrounding it, with a small group of young points in the companion galaxy. In the *B*-band, the old population is contributing 30% of the light, the intermediate-age population 46%, and the young population 24%.

The fit is quite poor in the nuclear region (point N), especially for the *V* and *R* bands. Examining the grid of models, there are two solutions which are almost equally acceptable for points in this region. The model shown in Figure 4 has an age of 128 Myr and a reddening $A_V = 2.0$ mag ($\chi^2_{\nu} = 1.7$); a second solution, with a reduced χ^2 only marginally higher ($\chi^2_{\nu} = 1.9$), has an age of 9 Myr and a reddening $A_V = 2.85$ mag. Since *BVRI* filters overlap and hence are not independent of each other, the χ^2_{ν} values cannot be taken as a quantitative measure of the goodness of

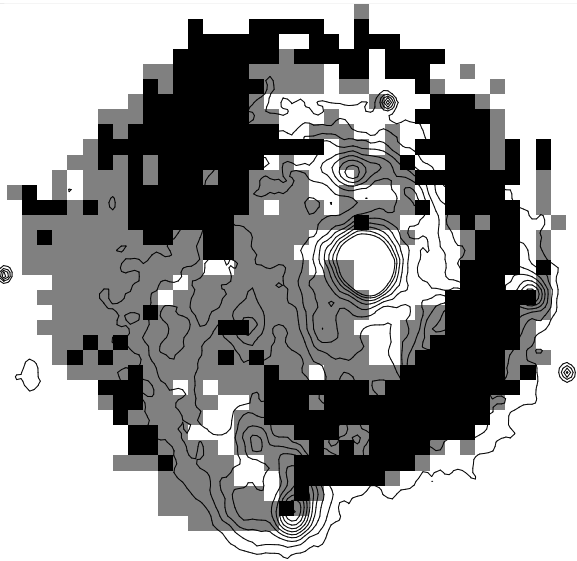


Figure 5. Age image of MRC B1221–423, created by fitting models with exponentially decaying star formation, with $\tau = 15$ Gyr and $\tau = 100$ Myr (see text for details). Pixels in the three peaks of the age histogram (Fig. 3) are shown as different colours. The oldest pixels (ages > 5 Gyr) are shown in black, pixels with ages between 80 Myr and 5 Gyr are shown as grey, and the young pixels (ages < 80 Myr) are shown as white. Contours of the B -band image are overlain for comparison. The ages of pixels clearly correlate with morphological features of the galaxy.

fit; however, the relative values indicate the second solution must be almost as good as the first.

The split between these two solutions can be seen in Figure 5, where some pixels in the nuclear region are white (young, with ages < 80 Myr), while others are grey (intermediate age, with ages between 80 Myr and 5 Gyr), despite having similar colours (Figure 2). This may well reflect a real mix of ages in the nuclear region, so that a single age population does not well describe the observed colours. Alternately, it could represent a spread in metallicity within the nuclear region, since changes in both age and metallicity can lead to similar colours.

The spectrum of the galaxy shows many emission lines (§ 3.3); however, as they are comparatively weak (contributing at most 7% of the flux), they do not seriously distort our analysis.

We also derive the extinction across the galaxy from the same model fits (Fig. 6). Most of the region has $A_V < 1$, but the centre of the galaxy and the blue regions to the west show evidence for large amounts of dust, $A_V \sim 1$ –2. This means that the region with the youngest population – the nucleus of the galaxy – requires the most internal reddening to fit the observed colours.

3.2 Surface photometry

Since B1221–423 is a powerful radio source, we would expect its host galaxy to be an elliptical galaxy; yet the optical image shows a galaxy which looks like a spiral. Analysis of

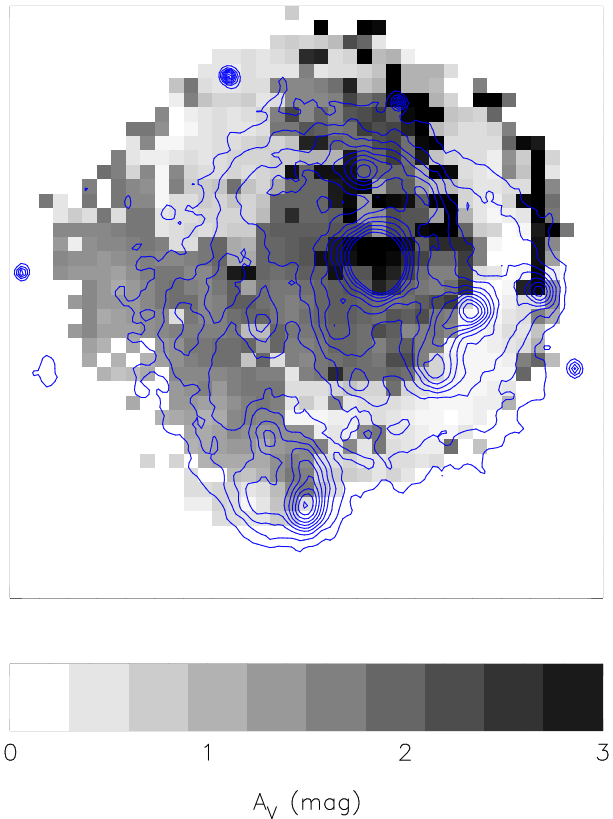


Figure 6. Extinction image of MRC B1221–423, from the same model fits as were used in Fig. 5. Black pixels correspond to heavily reddened regions, $A_V \geq 3$. Contours of the B -band image are overlain for comparison.

the light profile of the galaxy seemed to be the best way to identify the shape of the underlying stellar population.

We fit elliptical isophotes to the (unbinned) galaxy images, using the task `ellipse` in IRAF. We then attempted to fit either de Vaucouleurs $r^{1/4}$ -law profiles, appropriate for an elliptical bulge, or a combined bulge plus exponential disk profile, as expected for a spiral galaxy.

The results of the analysis are shown in Figure 7. The Ks -band image is well described by an $r^{1/4}$ -law profile, but the V and R -band profiles are not. This implies that the host galaxy does have a bulge, but it is being masked in bluer colours by the younger populations. We constrained the V and R -band profiles to have a bulge of the same size as the Ks -band, with an effective radius $R_e = 92$ pixels ($= 14.8$ arcsec). A de Vaucouleurs profile with this radius plus an exponential disk is a good fit to both the R and V -band light distributions (the R -band light profile is shown in Fig. 7). This bulge radius corresponds to a half-light radius of 42 kpc. Correcting for the extinction of $A_V = 1.9$ mag as derived in the SED fitting, and including K -corrections for the redshift $z = 0.17$ from Poggianti (1997), we can derive the intrinsic luminosity and colour of the bulge. The bulge has $V-K = 3.1$, and a luminosity in the V -band of $10^{12} L_\odot$.

3.3 Spectroscopy

We constructed a single spectrum (Fig. 8) by summing the spectral images from 2001, after aligning the spectra; we

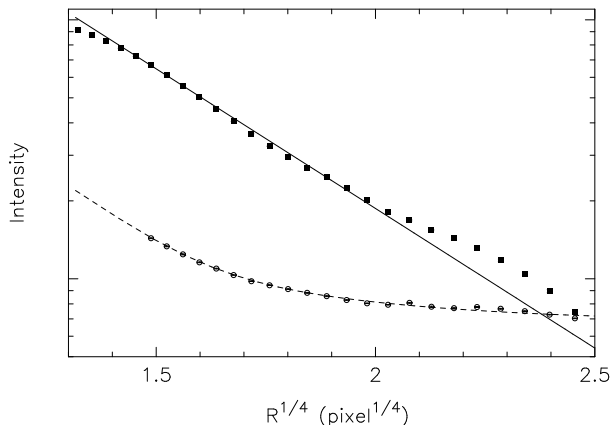


Figure 7. *Ks* (filled squares) and *R*-band (open circles) luminosity profiles for MRC B1221–423, plotted against $r^{1/4}$. The solid line shows the best-fitting de Vaucouleurs profile to the *Ks*-band data between 4 and 20 pixels ($1.4 < r^{1/4} < 2.1$). The dashed line shows a bulge+disk model fit to the *R*-band data, constraining the bulge to have the same radius as in the *Ks*-band, $R_e = 92$ pixels.

could only use the data from 2001 April 17 and 18 for the red spectrum, since we had a different wavelength setup for the first night (Table 1).

Emission is detected along the slit from the galaxy and companion. The heliocentric redshift of the emission lines, determined from a combined fit to the red side of the nuclear spectrum, is $z = 0.17068 \pm 0.00002$. The lines show significant rotation, with an amplitude of 90 km s^{-1} along this axis. The companion galaxy is found at a velocity of $-105 \pm 20 \text{ km s}^{-1}$ with respect to the nucleus. The line ratios can also clearly be seen to change along the slit, reversing from the nucleus to the companion, with the nuclear spectrum showing $\text{H}\alpha$ weaker than $[\text{N II}]$ ($\log [\text{N II}]/\text{H}\alpha = +0.25$), while in the companion $[\text{N II}]$ is weaker than $\text{H}\alpha$ ($\log [\text{N II}]/\text{H}\alpha = -0.35$).

We extracted the spectrum of the nuclear region by selecting the central two rows, corresponding to a linear size of 5.2 kpc. The resulting spectra are shown in Figure 8. The line properties were measured using the `specfit` package implemented in `IRAF` (Kriss 1994). Gaussian profiles were fitted to the lines, with a single velocity shift for all lines. The line fluxes and equivalent widths are given in Table 3.

A spectrum was extracted for the companion galaxy, by summing together seven rows at the position of the galaxy. This spectrum is also shown in Figure 8. This spectrum is clearly very different from the spectrum of the nuclear region, with much narrower lines and very different line ratios.

The nuclear spectrum shows the strong $[\text{O I}] \lambda 6300$, $[\text{O II}] \lambda 3727$ and $[\text{S II}] \lambda \lambda 6716, 6731$ emission lines characteristic of the class of active galactic nuclei known as “low-ionisation nuclear emission-line regions”, or LINERs (Heckman 1980). We can further investigate the classification of the different regions of the galaxy by using the classification diagrams of Veilleux & Osterbrock (1987).

From the ratio of the intensities of the $\text{H}\alpha$ and $\text{H}\beta$ lines, we can estimate the extinction towards the line-emitting regions. For the nucleus of the galaxy, the observed ratio is 10, compared with the expected ratio of 2.86 for a temperature $T = 10^4 \text{ K}$, which implies an extinction $A_V = 3.7 \text{ mag}$. For

the companion, the ratio $\text{H}\alpha/\text{H}\beta = 7.6$, which implies an extinction $A_V = 2.9 \text{ mag}$. These are both higher than the extinctions we derived from modelling the spectral energy distributions (Table 2), where we found $A_V = 1.9 \text{ mag}$ for the centre of the galaxy, and $A_V = 0.5 \text{ mag}$ for the companion (plus 0.33 mag of local extinction). However, since the companion has both Balmer emission and absorption, the ratio of $\text{H}\alpha$ to $\text{H}\beta$ may not be a reliable measure of the extinction.

The nucleus of MRC B1221–423 has the following line ratios, corrected for the reddening as determined from the Balmer decrement: $[\text{O I}]/\text{H}\alpha = 0.3$, $[\text{N II}]/\text{H}\alpha = 1.9$, $[\text{S II}]/\text{H}\alpha = 1.0$, and $[\text{O III}]/\text{H}\beta = 6.5$; these ratios match a LINER spectrum (Veilleux & Osterbrock 1987). The ratio of the $[\text{O III}]$ to $\text{H}\beta$ flux is higher than typical for a LINER spectrum, but since the $[\text{O III}]$ flux is not well determined (being seen only in the low-resolution spectrum from 2003 August) we give more weight to the high $[\text{N II}]/\text{H}\alpha$ ratio.

For the companion galaxy, the corrected line ratios are: $[\text{O I}]/\text{H}\alpha = 0.07$, $[\text{N II}]/\text{H}\alpha = 0.5$, $[\text{S II}]/\text{H}\alpha = 0.4$, and $[\text{O III}]/\text{H}\beta < -0.05$ (based on a marginal detection of $\text{H}\beta$ and an upper limit to $[\text{O III}]$), which match the spectrum of a starburst galaxy.

The limited signal-to-noise ratio of our spectra preclude a more detailed comparison with model population spectra, and do not allow us to make direct comparisons with the models derived from the broad-band images. However, there are a few indicators of the underlying stellar population which we can look at.

The $\lambda 4000\text{-\AA}$ break is a useful age-indicator for integrated stellar populations. Older populations produce a discontinuity at 4000\AA due to the increase in stellar opacity produced by metal lines shortward of 4000\AA in late-type stars. We measured the $\lambda 4000\text{-\AA}$ break index by comparing the mean flux density in two windows above and below 4000\AA , taking the ratio of the mean flux between 4050 and 4250\AA with the mean flux between 3750 and 3950\AA (Bruzual 1983). For the nuclear spectrum, this index is 1.37. This small break index confirms the existence of recent star formation in the nucleus of the galaxy (e.g. Kauffmann et al. 2003).

Since the galaxy contains a powerful radio source, some fraction of the excess blue light may arise from the AGN. We detect the G band in the nuclear spectrum, with an equivalent width of 4.1\AA (Table 3), which is consistent with the values seen in normal elliptical galaxies (e.g. Trager et al. 1998); this means that we are definitely detecting stars. The detection of $\text{H}\delta$ absorption, with an equivalent width of 1.2\AA means that at least some of the blue excess is being contributed by intermediate-age stars. We conclude that it is unlikely that the AGN contributes more than about 50% of the light.

4 CONCLUSIONS

We have shown that the host galaxy of MRC B1221–423 and its interacting companion can be resolved into different stellar populations. We have achieved this in two different ways, using colour-magnitude diagrams, and by using models for the spectral energy distribution of individual pixels. Both these methods separate the pixels into distinct regions

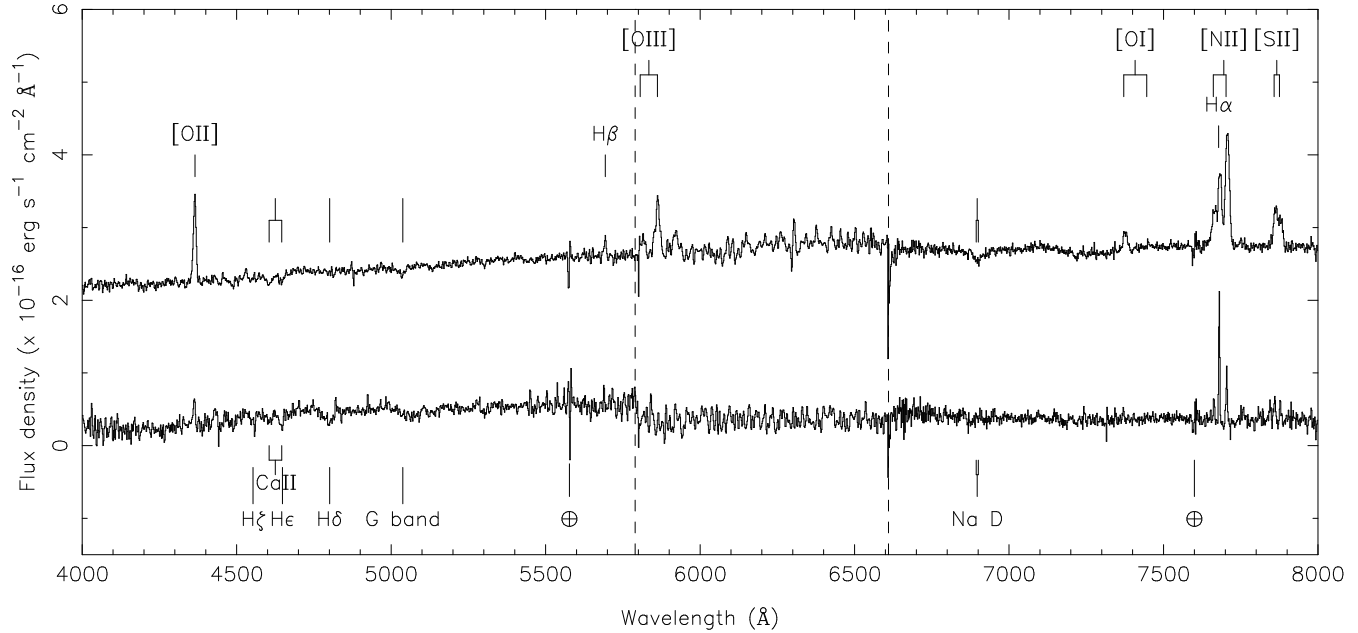


Figure 8. Combined spectrum of the nucleus (top spectrum) and the companion (bottom spectrum), with emission and absorption lines identified. The nuclear spectrum has been offset in the y -direction by $2 \times 10^{-16} \text{ erg s}^{-1} \text{ cm}^{-2} \text{ \AA}^{-1}$ for clarity. The region between the dashed lines is the lower resolution spectrum from 2003 August, which has much lower signal to noise; the data on either side are the high-quality summed spectra taken in 2001 April from the blue and red arms of the spectrograph.

Table 3. Properties of detected emission lines and absorption lines in the spectra of the nucleus and companion galaxy (Fig. 8). The columns show the line with its rest wavelength, its equivalent width, integrated flux, and FWHM for the nuclear and companion spectra respectively. Line properties were measured by fitting Gaussian profiles to the spectra; the values in the table are the properties of the fitted Gaussians. The quantities with no errors (shown in italics) are linked to the corresponding quantities of another line, e.g. the flux ratio of the [O II] $\lambda\lambda 3727, 3729$ lines was fixed at 4.3, and their FWHMs constrained to be the same. Negative values denote emission lines. The [O III] $\lambda\lambda 5007, 4959$ lines (marked with *) were present only in the low-resolution spectrum of 2003 August. Lines which were not detected are indicated by a $3\text{-}\sigma$ upper limit in the equivalent width column, calculated by $\text{EW}_{\text{lim}} = 3\sqrt{2} \Delta\lambda / \text{SNR}$, where $\Delta\lambda$ is the dispersion ($\text{\AA}/\text{pix}$) and SNR is the signal-to-noise ratio of the spectrum at the location of the line; limits on doublets are shown as a single entry.

| Line | Nucleus | | | Companion | | |
|-----------------|------------------------|--|--------------------------------|------------------------|--|--------------------------------|
| | EW (\AA) | Flux density ($\times 10^{-16}$ $\text{erg s}^{-1} \text{ cm}^{-2}$) | FWHM (km s^{-1}) | EW (\AA) | Flux density ($\times 10^{-16}$ $\text{erg s}^{-1} \text{ cm}^{-2}$) | FWHM (km s^{-1}) |
| [O II] 3727 | -40.9 ± 1.1 | -7.3 ± 0.2 | 685 ± 20 | -7.5 ± 1.4 | -2.2 ± 0.4 | 500 ± 130 |
| [O II] 3729 | <i>-9.4</i> | <i>-1.7</i> | <i>685</i> | <i>-1.8</i> | <i>-0.5</i> | <i>500</i> |
| H β 4861 | -3.1 ± 0.9 | -1.3 ± 0.4 | 360 ± 120 | -1.9 ± 1.0 | -1.0 ± 0.6 | 190 ± 150 |
| [O III] 4959* | <i>-4.3</i> | <i>-3</i> | <i>800</i> | < 6 | - | - |
| [O III] 5007* | -12.9 ± 1.6 | -9 ± 1 | 800 ± 110 | < 6 | - | - |
| [O I] 6300 | -4.9 ± 0.5 | -3.4 ± 0.4 | 560 ± 60 | < 0.7 | - | - |
| [N II] 6548 | <i>-11.1</i> | <i>-8.5</i> | <i>580</i> | <i>-3.3</i> | <i>-1.2</i> | <i>170</i> |
| H α 6563 | -21.0 ± 0.9 | -13.8 ± 0.4 | 480 ± 20 | -18.0 ± 0.7 | -7.6 ± 0.3 | 145 ± 6 |
| [N II] 6583 | -33.2 ± 0.6 | -25.3 ± 0.6 | 580 ± 15 | -9.8 ± 0.6 | -3.6 ± 0.3 | 170 ± 15 |
| [S II] 6716 | -11.2 ± 0.5 | -8.3 ± 0.4 | 560 ± 30 | -5.2 ± 0.9 | -1.9 ± 0.3 | 200 ± 30 |
| [S II] 6730 | -8.0 ± 0.5 | -5.9 ± 0.4 | <i>560</i> | -3.8 ± 0.7 | -1.4 ± 0.3 | <i>200</i> |
| Ca II H 3933 | 5.8 ± 0.7 | 1.3 ± 0.1 | 1080 ± 130 | 3.5 ± 1.9 | 1.4 ± 0.8 | 790 ± 420 |
| Ca II K 3968 | <i>5.8</i> | <i>1.4</i> | <i>1080</i> | <i>3.5</i> | <i>1.9</i> | <i>790</i> |
| H ζ 3889 | < 1.1 | - | - | 3.2 ± 1.8 | 1.3 ± 0.7 | <i>860</i> |
| He 3970 | < 0.9 | - | - | < 1.5 | - | - |
| H δ 4101 | 1.2 ± 0.8 | 0.3 ± 0.2 | <i>1080</i> | 5.5 ± 1.8 | 2.5 ± 0.8 | 860 ± 180 |
| G band 4304 | 4.1 ± 0.7 | 1.2 ± 0.2 | <i>1080</i> | < 0.7 | - | - |
| Na D1 5889 | 1.5 ± 0.3 | 1.0 ± 0.2 | 620 ± 180 | < 0.8 | - | - |
| Na D2 5895 | <i>0.8</i> | <i>0.5</i> | <i>620</i> | < 0.8 | - | - |

with different colours and/or ages. We interpret this as indicating that the galaxy and its companion have undergone several episodes of star formation, possibly associated with the tidal interaction between the two.

The ages we deduce for the stellar population fall into three distinct groups. An old population, with age $t \sim 15$ Gyr, occupies the outskirts of the host galaxy. An intermediate age population, with $t \sim 300$ Myr, is found near the nucleus and around the tidal tail joining the two galaxies, while the youngest population, with ages less than 10 Myr, is concentrated in the nucleus and the blue regions to the west, as well as in the companion galaxy.

The location of these populations is not identical to the separation suggested by the regions in the colour-magnitude diagram (Figure 2). This may be due to the effects of dust, which our SED modelling suggests is concentrated in the nucleus of the host galaxy.

The relationship of the different stellar populations with the underlying powerful radio source is much less clear. The age of the source, estimated from the power of the radio jets and total stored energy in the synchrotron plasma of the lobes (Rawlings & Saunders 1991), is only 10^5 yr (Safouris et al. 2003). This is much younger than the youngest population we detected, with an age of about 10 Myr (Section 3.1.2), and suggests there must be a substantial time delay between the most recent burst of star formation and the triggering of the radio source.

A possible scenario to explain the three component populations is as follows: the tidal interaction began 300 Myr ago, which triggered star formation in both the host galaxy and the companion. We see the results of this episode of star formation as the intermediate-age population. Gas is driven down into the nucleus on timescales of $\sim 10^8$ yr, where it both cools to form stars, which we see as the 10 Myr-old population, and triggers activity in the central supermassive black hole. Delays of this order are predicted in theoretical calculations, (e.g. Lin et al. 1988), which give time delays of a few $\times 10^8$ yr between the tidal interaction and the gas reaching the centre of the galaxy.

This would be classed as a “minor merger”, involving interaction of the galaxy with a dwarf satellite. Such interactions have been shown to be effective in feeding material into the nuclear regions (Hernquist & Mihos 1995). This scenario for B1221–423 would fit with the idea that low redshift radio galaxies are triggered by material falling into a pre-existing supermassive black hole, in contrast with very high redshift radio galaxies and quasars, which are often associated with major mergers and the simultaneous formation of a massive bulge and the central black hole.

We thank Oliver Prouton for obtaining the optical images of B1221–423, and the anonymous referee for helpful comments. RWH and EMS acknowledge support for this project from the Australian Research Council and the University of Sydney Sesqui grant scheme.

REFERENCES

Abraham R. G., Ellis R. S., Fabian A. C., Tanvir N. R., Glazebrook K., 1999, MNRAS, 303, 641
 Barnes J. E., Hernquist L., 1992, ARA&A, 30, 705
 Bennett A. S., 1962, MmRAS, 68, 163

Bessell M. S., 1990, PASP, 102, 1181
 Best P. N., Longair M. S., Röttgering H. J. A., 1996, MNRAS, 280, L9
 Bolzonella M., Miralles J.-M., Pelló R., 2000, A&A, 363, 476
 Bothun G. D., 1986, AJ, 91, 507
 Bruzual A. G., 1983, ApJ, 273, 105
 Bruzual A. G., Charlot S., 1993, ApJ, 405, 538
 Conway J. E., 2002, NewAR, 46, 263
 Croke B. F. W., 1995, PASP, 107, 1255
 de Grijs R., Lee J. T., Clemencia Mora Herrera M., Fritzev. Alvensleben U., Anders P., 2003, NewA, 8, 155
 Fanti R., Fanti C., Schilizzi R. T., Spencer R. E., Rendong N., Parma P., van Breugel W. J. M., Venturi T., 1990, A&A, 231, 333
 Gunn J. E., Stryker L. L., 1983, ApJS, 52, 121
 Heckman T. M., 1980, A&A, 87, 152
 Hernquist L., Mihos J. C., 1995, ApJ, 448, 41
 Kaiser C. R., Alexander P., 1997, MNRAS, 286, 215
 Kassin S. A., Frogel J. A., Pogge R. W., Tiede G. P., Sellgren K., 2003, AJ, 126, 1276
 Kauffmann, G., Heckman, T. M., White, S. D. M., Charlot, S., Tremonti, C., Peng, E. W., Seibert, M., Brinkmann, J., Nichol, R. C., Subba Rao, M., York, D. 2003, MNRAS, 341, 54
 Kong X., Zhou X., Chen J., Cheng F., et al. 2000, AJ, 119, 2745
 Kriss G. A., 1994, in Crabtree D. R., Hanisch R. J., Barnes J., eds, Astronomical Data Analysis Software and Systems III Vol. 61 of ASP Conference Series, Fitting models to UV and optical spectra using SPECFIT in IRAF. ASP, San Francisco, pp 437–446
 Landolt A. U., 1992, AJ, 104, 340
 Large M. I., Mills B. Y., Little A. G., Crawford D. F., Sutton J. M., 1981, MNRAS, 194, 693
 Lin D. N. C., Pringle J. E., Rees M. J., 1988, ApJ, 328, 103
 Longair M. S., Best P. N., Röttgering H. J. A., 1995, MNRAS, 275, L47
 O’Dea C. P., 1998, PASP, 110, 493
 Persson S. E., Murphy D. C., Krzeminski W., Roth M., Rieke M. J., 1998, AJ, 116, 2475
 Poggianti B. M., 1997, A&AS, 122, 399
 Rawlings S., Saunders R., 1991, Nat, 349, 138
 Readhead A. C. S., Taylor G. B., Pearson T. J., Wilkinson P. N., 1996, MNRAS, 460, 634
 Rieke G. H., Lebofsky M. J., 1985, ApJ, 288, 618
 Safouris V., Hunstead R. W., Prouton O. R., 2003, Proc. Astron. Soc. Aust., 20, 1
 Scheuer P. A. G., 1974, MNRAS, 166, 513
 Schlegel D. J., Finkbeiner D. P., Davis M., 1998, ApJ, 500, 525
 Simpson C., Clements D. L., Rawlings S., Ward M., 1993, MNRAS, 262, 889
 Trager S. C., Worthey G., Faber S. M., Burstein D., González J. J., 1998, ApJS, 116, 1
 Veilleux S., Osterbrock D. E., 1987, ApJS, 63, 295